Journal of Earthquake Engineering
Publication details, including instructions for authors and subscription information:
http://www.tandfonline.com/loi/ueqe20

LIQUEFACTION-INDUCED SETTLEMENT OF SHALLOW FOUNDATIONS AND REMEDIATION: 3D NUMERICAL SIMULATION

AHMED ELGAMAL [a], JINCHI LU [a] & ZHAOHUI YANG [a]

[a] Department of Structural Engineering, University of California, San Diego, La Jolla, CA 92093, USA

Available online: 15 Sep 2009

To cite this article: AHMED ELGAMAL, JINCHI LU & ZHAOHUI YANG (2005): LIQUEFACTION-INDUCED SETTLEMENT OF SHALLOW FOUNDATIONS AND REMEDIATION: 3D NUMERICAL SIMULATION, Journal of Earthquake Engineering, 9:S1, 17-45

To link to this article: http://dx.doi.org/10.1080/13632460509350578

Journal of Earthquake Engineering
Vol. 9, Special Issue 1 (2005) 17–45

Imperial College Press
www.icpress.co.uk

LIQUEFACTION-INDUCED SETTLEMENT OF SHALLOW FOUNDATIONS AND REMEDIATION: 3D NUMERICAL SIMULATION

AHMED ELGAMAL, JINCHI LU and ZHAOHUI YANG
Department of Structural Engineering
University of California, San Diego, La Jolla, CA 92093, USA

Calibrated Finite Element (FE) simulations are increasingly providing a reliable environment for modelling liquefaction-induced ground deformation. Effects on foundations and super-structures may be assessed and associated remediation techniques may be explored, within a unified framework. Current capabilities of such a FE framework are demonstrated via a simple 3-dimensional (3D) series of simulations. Ground liquefaction and settlement under the action of a surface load is investigated. Liquefaction hazard mitigation is explored by soil compaction and/or increase of permeability below and around the applied surface load. The potential and limitations of numerical simulation are discussed, along with future research needs and challenges towards more reliable practical application.

Keywords: Liquefaction-induced settlement; numerical simulations; shallow foundations; site remediation; FE simulations.

1. Introduction

Finite element modelling along with other numerical simulation techniques has been providing valuable insights into the response of ground and ground/foundation/structure systems. In the early 1990s, liquefaction behaviour mechanisms and numerical simulation were addressed within a concerted effort, on the basis of more than 10 different centrifuge testing experimental setups [Arulanandan and Scott, 1993, 1994]. Overall, some success was achieved, but significant challenges were evident both numerically and experimentally. Following this effort, much research has been conducted, with 3 main outcomes:

(1) Our understanding and appreciation of the underlying liquefaction-induced deformation mechanisms has steadily increased in view of continued experimentation and evidence from the increasing database of post-earthquake reconnaissance studies [e.g. JGS, 1996, 1998; EERI, 2000]. Notable among such issues are:

   (i) Further appreciation of the significance of cyclic mobility in dictating deformations in clean cohesionless soils [e.g. Holzer *et al.*, 1989; Zeghal and Elgamal, 1994],

(ii) The important contribution of permeability towards the process and extent of deformation accumulation [e.g. Yang and Elgamal, 2002; Sharp *et al.*, 2003],

(iii) The influence of fines-content (non-plastic) and the associated potential detrimental effect [e.g. Bray *et al.*, 2004],

(iv) Influence of permeability interfaces [e.g. Kokusho, 1999; Malvick *et al.*, 2004] and situations where major lateral deformations may accumulate along relatively narrow seams at such locations (e.g. in commonly encountered hydraulic-fill formations, and in alluvial deposits), and

(v) The impact of an overlying structure and its foundation, and the effect thereof on the near field behaviour and ensuing deformation pattern [e.g. Liu and Dobry, 1997; Hausler, 2002].

(2) Continued development and calibration of the numerical simulation tools. Among the primary issues are:

(i) Calibration of soil model properties using acceleration and pore-pressure data from centrifuge and shake-table experiments, as well as seismic records from *in-situ* downhole accelerometer/pore-pressure arrays [e.g. Elgamal *et al.*, 2001],

(ii) Development of constitutive models that put more emphasis on cyclic mobility effects as observed from experimental data on clean sands [e.g. Iai, 1991; Kramer and Elgamal, 2001; Elgamal *et al.*, 2003],

(iii) Pilot studies on engineering approaches to account for effect of permeability interfaces in stratified layered soils [e.g. Yang and Elgamal, 2002],

(iv) Steady improvements in procedures for modeling large-deformation scenarios [e.g. Manzari, 2004],

(v) Emerging efforts to include uncertainty and sensitivity in the analysis framework [e.g. Conte *et al.*, 2003; Gu and Conte, 2003; Borja, 2004], and most importantly,

(vi) The increasing adoption and use of elaborate simulations which more accurately represent geometry and deformation mechanisms of complex geotechnical systems [e.g. Pecker *et al.*, 2001; Ju, 2004; Lu *et al.*, 2004].

(3) Advances in software and hardware. Among the issues impacting liquefaction simulation are:

(i) Wider availability of affordable personal computer workstations with large memory (e.g. 2 and 3 Gigabyte RAM), faster processors (3 Gigahertz), etc., allowing users to conduct higher fidelity analyses (2D and 3D),

(ii) Gradual developments in parallel computing hardware in the form of affordable networked PC workstations enabling the order of 1 million degree-of-freedom models [e.g. Jeremic, 2004],

(iii) Wider availability of mesh generation and visualisation software packages such as GID [CIMNE, 1999],

(iv) Recent availability of large-scale collaborative open-source codes for seismic analysis including advanced modelling capabilities for soil and structural elements [at the forefront of such efforts is the Berkeley framework OpenSees http://opensees.berkeley.edu, McKenna and Fenves, 2001], and

(v) Facilitated development of user friendly interfaces that greatly simplify development of meshes, selection of material properties, execution of calculations, and visualisation of results [e.g. Pro-shake code http://www.proshake.com, http://cyclic.ucsd.edu, http://cyclic.ucsd.edu/cyclictp, and http://cyclic.ucsd.edu/openseestp, Elgamal *et al.*, 2004], and as well as current efforts in archiving and database access [e.g. Peng *et al.*, 2003].

In addition to the above, we are on the cusp of a new cycle of national and international collaborative developments within frameworks such as the Network of Earthquake Engineering Simulation (NEES, http://www.nees.org), and the new Japan e-defense shaking-table facility (http://www.bosai.go.jp/sougou/sanjigen/3De/index.htm). These new experimental facilities and the associated numerical modelling efforts will eventually lead to consensus documents regarding liquefaction mechanisms and appropriate computational simulation environments. Numerical simulation will rapidly become an integral component providing valuable insights for design purposes, where substantial safety and economical concerns are at stake.

In the following sections, an attempt is made to demonstrate current computational capabilities in the domain of ground modification for seismic liquefaction applications. In particular, valuable insights can now be gained in view of: (i) Availability of calibrated constitutive models, and (ii) practical feasibility of conducting more accurate 3D analyses within a comparative framework. In order to demonstrate the above, a simple analysis framework will be adopted. The aim here is to assess potential, and derive conclusions, as to efficiency and availability for wide use. For that purpose, the problem of ground modification for mitigation of liquefaction effects due to surface loads will be addressed. Overall comparison of the numerically observed patterns with experimental observations is shown to demonstrate promise and value.

2. Shallow Foundations on Liquefiable Soil

Liquefaction-induced tilting and settlement of buildings on shallow foundations results in significant damage, disruption of function, and considerable replacement expense. This type of response was commonplace with much being documented during Niigata, Japan 1964; Dagupan City, Philippines, 1990; Chi-Chi, Taiwan, 1999; and Koaleci, Turkey, 1999 [Kishida, 1966; Ohsaki, 1966; Seed and Idriss, 1967; Yoshimi and Tokimatsu, 1977; Adachi *et al.*, 1992; Ishihara *et al.*, 1993; Tokimatsu *et al.*, 1991, 1994; EERI, 2000, 2001].

Liu and Dobry [1997] conducted a centrifuge investigation related to the problem of shallow-foundation liquefaction-induced settlement. In prototype scale, they

explored the response of an essentially rigid footing (about 4–5 m diameter) supported on liquefiable sand (D_r of about 50%, with 10 m to 12.5 m saturated layer thickness). In this study, the mitigation of liquefaction hazard was explored with emphasis on compaction and permeability variation of the immediate ground below the foundation. More recently Haulser [2002] conducted a multi-experiment centrifuge study where ground improvement by compaction was explored. Scenarios of different soil relative density, and compaction to different depths below the superstructure were explored.

Our numerical investigation addresses the effect of compaction with and without permeability increase. No direct comparisons are made with centrifuge studies, but observed trends are assessed and discussed. In this regard, the computational framework can be an environment for development of insights that must be further substantiated by experimental/full-scale observation.

3. Finite Element Formulation

Herein, the program CYCLIC [Parra, 1996; Yang, 2000; Yang *et al.*, 2003] is used in its 3D version [Lu, 2005]. The soil domain is represented by 20–8 node, effective-stress fully coupled (solid-fluid) brick elements [Lu, 2005]. In this formulation, 20 nodes describe the solid translational degrees of freedom, and 8 nodes describe the fluid pressure (details are provided in Appendix).

A key component of this modelling effort lies in earlier calibration of the employed soil model (based on recorded response of Nevada Sand at D_r of about 40%) under situations of liquefaction and lateral spreading response [Parra, 1996; Yang, 2000; Elgamal *et al.*, 2003; Yang *et al.*, 2003; Yang and Elgamal, 2004]. The compacted zone modelling parameters were chosen mainly based on extrapolating the $D_r = 40\%$ calibration results, available empirical formulae [Kramer, 1996], and engineering judgement. While more verification and further tuning is always possible and potentially helpful, the model currently reproduces salient liquefaction response characteristics, based on earlier calibration work over the past 10 years [Parra, 1996; Yang, 2000; Yang *et al.*, 2003; Yang and Elgamal, 2004]. Details of the employed numerical formulation framework are included in the Appendix, along with the associated numerical modelling parameters.

4. Shallow Foundation Model

A 10 m saturated medium sand layer was studied (based on Nevada Sand at D_r of about 40%). Herein, the load (40 kPa, or about 2 m of an equivalent soil overburden) was simply applied at ground level in the form of a distributed surficial vertical stress over a 2 m×2 m area (Fig. 1). More accurate loading patterns may be explored in future studies with no added complexity (e.g. imposing load that represents an actual building geometry by using additional super-structure elements, modelling

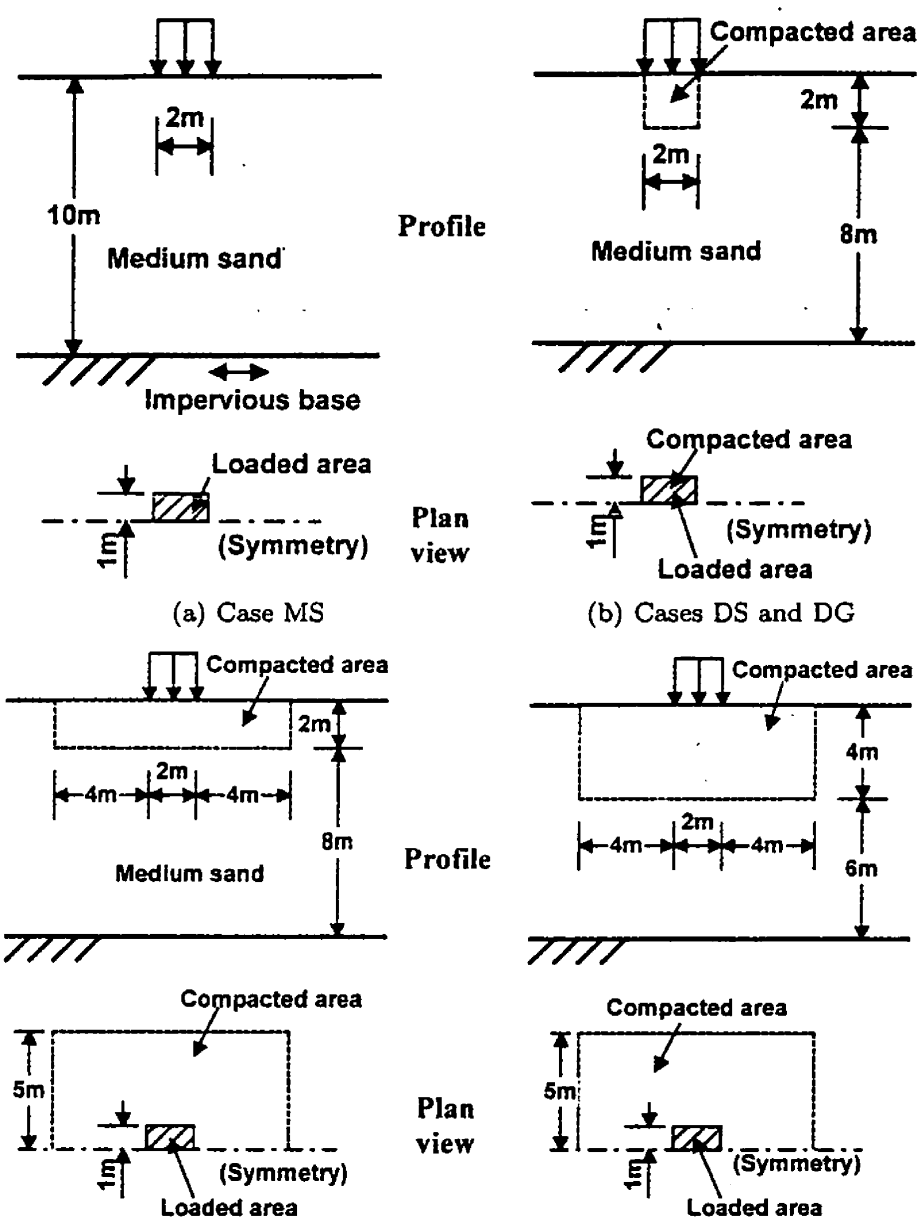

Fig. 1. A medium sand soil layer subjected to a surface load of 40 kPa.

of potential embedment of the foundation below ground surface, and/or locating water table at some depth below ground surface).

In view of symmetry, a half-mesh (75 elements in total) is studied as shown in Fig. 2. Length in the longitudinal direction is 26 m, with 13 m transversally (in this half-mesh configuration). At this preliminary stage, the employed mesh is crude geometrically, and further refinement is addressed later. The following (solid and fluid) boundary conditions were implemented: (i) Lateral excitation was defined along the base in the longitudinal direction (x-axis), (ii) at any given depth, displacement degrees of freedom of the left and right boundaries were tied together (both horizontally and vertically using the penalty method) to reproduce a 1D shear wave propagation mechanism effect, (iii) the soil surface was traction free,

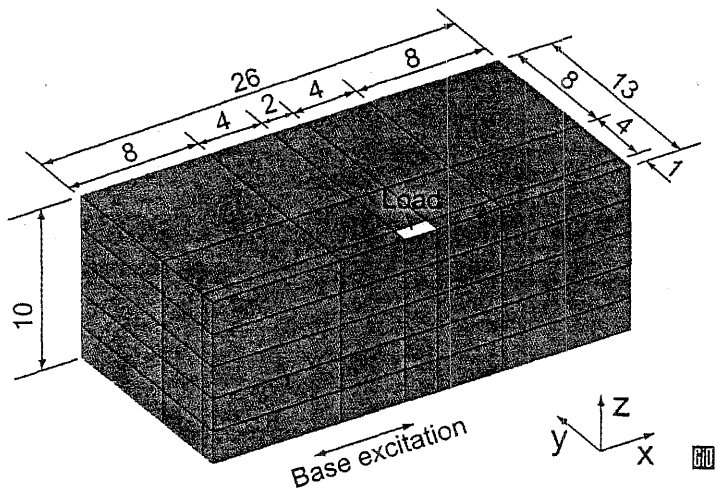

Fig. 2. Finite element mesh.

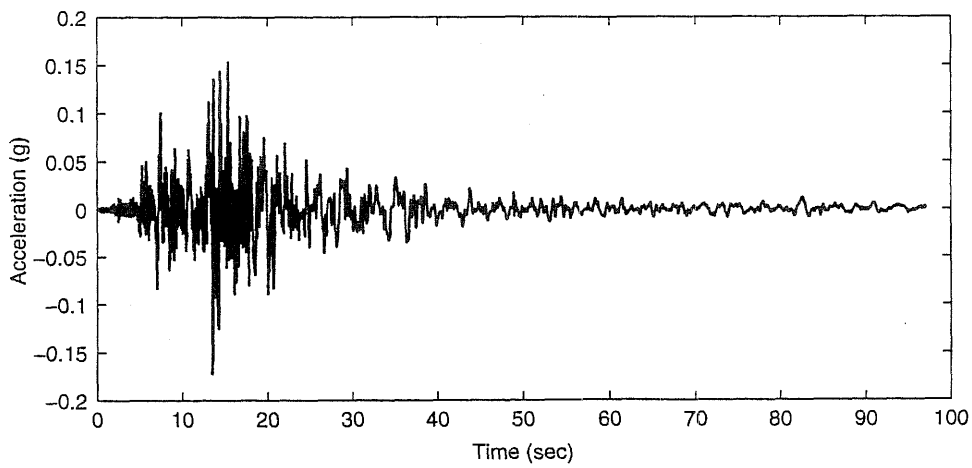

Fig. 3. Base input motion.

with zero prescribed pore pressure, and (iv) the base and lateral boundaries were impervious.

The 7.5 m depth (NS direction) downhole acceleration record (Fig. 3) from the Wildlife site during the 1987 Superstition Hills earthquake was employed as base excitation along the x-axis. During this event, much evidence of liquefaction was observed at Wildlife [Holzer *et al.*, 1989; Youd and Holzer, 1994]. Selection of this excitation (recorded at 7.5 m depth) as one representative motion causing liquefaction is suitable for our demonstration purposes, but an appropriate ensemble of records should be used to develop more comprehensive conclusions.

Table 1. Preliminary crude mesh simulations.

Simulation	Compacted area (m × m × m)	Compacted area permeability k (m/s)	Foundation settlement (m)
MS1D (Medium Sand, 1D)	(Site response simulation)		0.00
MS (Medium Sand)	Benchmark, no compaction (Fig. 1a)		0.23
DS (Dense Sand)	2 × 2 × 2 (Fig. 1b)	6.6×10^{-5}	0.22
DG (Dense Gravel)	2 × 2 × 2 (Fig. 1b)	1.0×10^{-2}	0.15
DSL (Dense Sand, Large area)	10 × 10 × 2 (Fig. 1c)	6.6×10^{-5}	0.26
DGL (Dense Gravel, Large area)	10 × 10 × 2 (Fig. 1c)	1.0×10^{-2}	0.07
DSL4 (Dense Sand, Large area, 4 m depth)	10 × 10 × 4 (Fig. 1d)	6.6×10^{-5}	0.24
DGL4 (Dense Gravel, Large area, 4 m depth)	10 × 10 × 4 (Fig. 1d)	1.0×10^{-2}	0.02

5. Site Remediation

We attempt to explore the effect of including a compacted zone below the loaded area. Employing high permeability drains (e.g. wick drains) or replacing the original sand (permeability $k = 6.6 \times 10^{-5}$ m/s) under the load with a high permeability compacted gravel ($k = 1.0 \times 10^{-2}$ m/s) was also explored. In both cases, the treated zone was varied in depth and lateral extent.

Table 1 depicts the scope of our ground modification study (Fig. 1). Specifically, a total of eight simulations were performed. Case **MS1D** (Table 1) simulates a Medium Sand site response situation (1D shear wave propagation) with no applied surface load. The result obtained provides a reference of free-field response for the remaining cases. Case **MS** is the same as **MS1D** with the surface load applied (Table 1 and Fig. 1(a)). This is the case without any remediation serving as the benchmark. Cases **DS**, **DSL** and **DSL4** (Figs. 1(b), (c) and (d)) are studied to evaluate the effect of compaction (**D**ense **S**and) for different levels of soil depth and lateral extent. Cases **DS** and **DSL** are both compacted to 2 m depth (Figs. 1(b) and (c)) while a Larger 10 m lateral extent is compacted in Case **DSL** (compared to 2 m width in Case DS). Case DSL4 (Fig. 1(d)) is the same as Case DSL with compaction of up to 4 m. Gravel permeability is used for the compacted area in Cases **DG**, **DGL** and **DGL4**.

6. Simulated Foundation Settlement

Figure 4 displays the foundation settlement time histories for all conducted simulations. The final settlements are also listed in Table 1. It is seen that compaction to a larger depth and/or greater lateral extent had a minor effect on reducing foundation settlement (Cases DS, DSL and DSL4). However, higher permeability of the compacted area played a key role in decreasing settlement. In the case of DGL4 (dense gravel, 10 m wide and 4 m deep), the foundation final settlement (Table 1) was reduced to 0.02 m (compared to 0.23 m in Case DSL4).

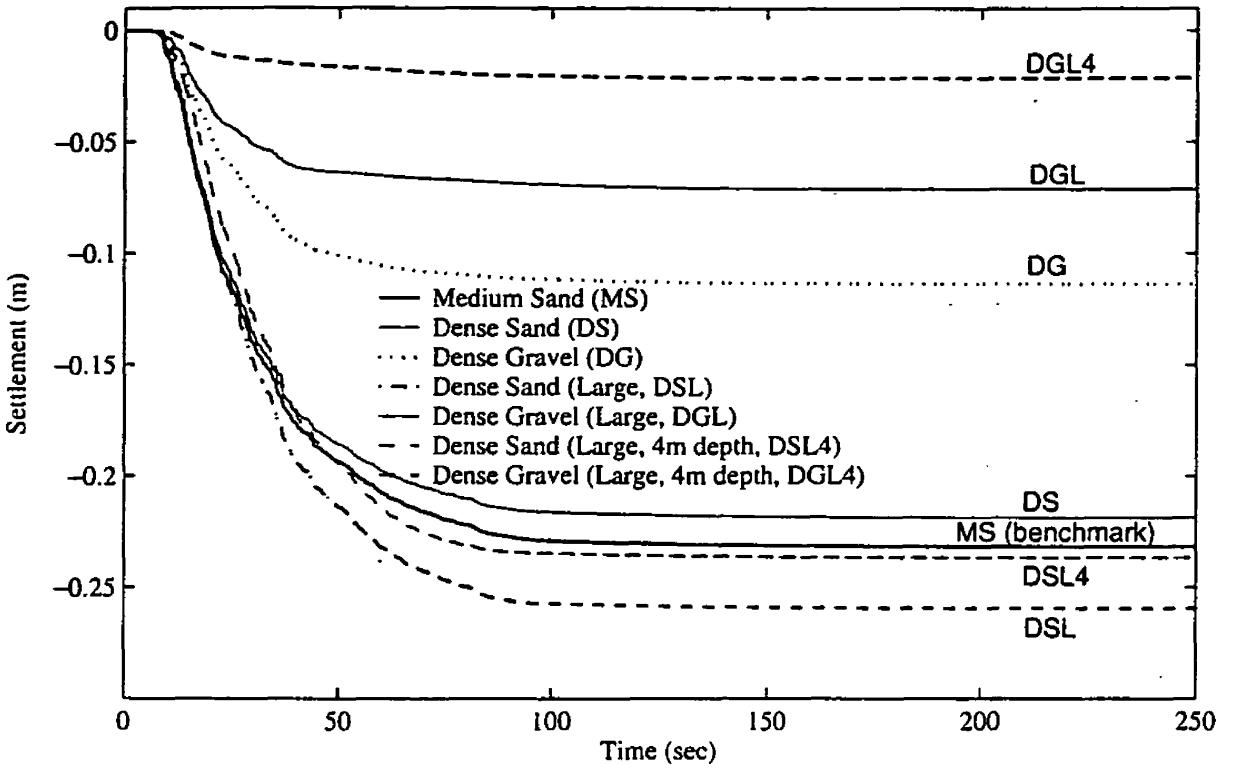

Fig. 4. Foundation settlement time histories.

Additional observations for compaction effects (Table 1):

(i) In the investigated scenario, the zone treated by compaction was virtually of no consequence. Such an outcome remains to be verified by additional simulations and experiments.
(ii) In fact, increasing the compacted area (case of 2 m depth, DSL) actually resulted in an increased settlement which is a counter-intuitive outcome. It appears that the compacted area acted as an embedded block, ultimately resulting in a marginally larger liquefaction-induced settlement.
(iii) As expected, compaction to depths greater than 4 m (e.g. compacting throughout the entire depth, in Lu, 2005) was found to lower the total settlement by about 50% (not shown).

Increased permeability effects (Table 1):

(i) High permeability right under the foundation only (DG) immediately reduced the settlement by more than 50%.
(ii) Increasing the treated zone laterally (DGL), then also vertically (DGL4) eventually resulted in an order of magnitude of settlement reduction.

Details and insights regarding the underlying dynamic response mechanisms are discussed next.

7. Response Characteristics and Discussion

7.1. *Site response (Case MS1D)*

Figures 5 and 6 display lateral acceleration and excess pore pressure (u_e) time histories at different depths for Case MS1D. Figure 6 shows that the entire sand stratum was liquefied throughout (maximum excess pore-pressure u_e equals the initial overburden vertical effective stresses σ'_{v0}, i.e. the pore-pressure ratio $r_u = u_e/\sigma'_{v0} = 1.0$). Initial liquefaction was reached at 9 seconds near the surface (Fig. 6), propagating downwards throughout the stratum after about 13 seconds of excitation (Fig. 6). As liquefaction occurred, acceleration at relatively high levels of input excitation (during 10–20 s) was clearly attenuated (Fig. 5).

Once liquefaction was reached, r_u remained at 1.0 with reduction only taking place near the end of shaking, from the base upwards. The stress-paths and stress-strain history of Fig. 7 show the typical mechanism of cyclic decrease in effective confinement due to pore-pressure buildup, along with the associated loss in shear stiffness and strength.

7.2. *Benchmark simulation (Case MS)*

In the free field (not shown), the response was essentially the same as that of MS1D. Under the foundation, strong dilative response was observed. As shown in Fig. 8, a number of instantaneous sharp pore pressure drops occurred. This dilative response is also observed in the stress paths as shown in Fig. 9. In the soil section immediately below the foundation, u_e buildup was relatively slow (top graph of Fig. 8). This pattern of response was caused mainly by the shear-induced dilative response during the deformation of the saturated soil below the foundation [Liu and Dobry, 1997; Adalier *et al.*, 1998]. As the rate of settlement decreased (MS in Fig. 4), u_e under the foundation (top graph of Fig. 8) built up rapidly and only started to dissipate after nearly reaching liquefaction at about 110 seconds (well after the end of shaking at 98 seconds). The permanent foundation settlement was 0.23 m (Table 1) in Case MS. Similar characteristics of u_e response were recorded during the centrifuge test of Liu and Dobry (corner of Fig. 8).

7.3. *Compaction remediation*

Cases DS, DSL and DSL4 were compacted to different lateral extent and soil depth levels (Table 1 and Fig. 1). The response recorded away from the foundation (free-field) in all these cases was quite similar to that of Case MS (not shown). Under the foundation, the response (e.g. lateral acceleration and excess pore pressure time histories) in cases DS, DSL and DSL4 were also quite comparable to Case MS.

Pore-pressure for DSL4 under the foundation is shown in Fig. 10. Note the similarity to MS (Fig. 8), with u_e rising near the end of shaking (even at 4 m and 6 m depth in DSL4), and the somewhat faster dissipation of u_e at 8 m depth.

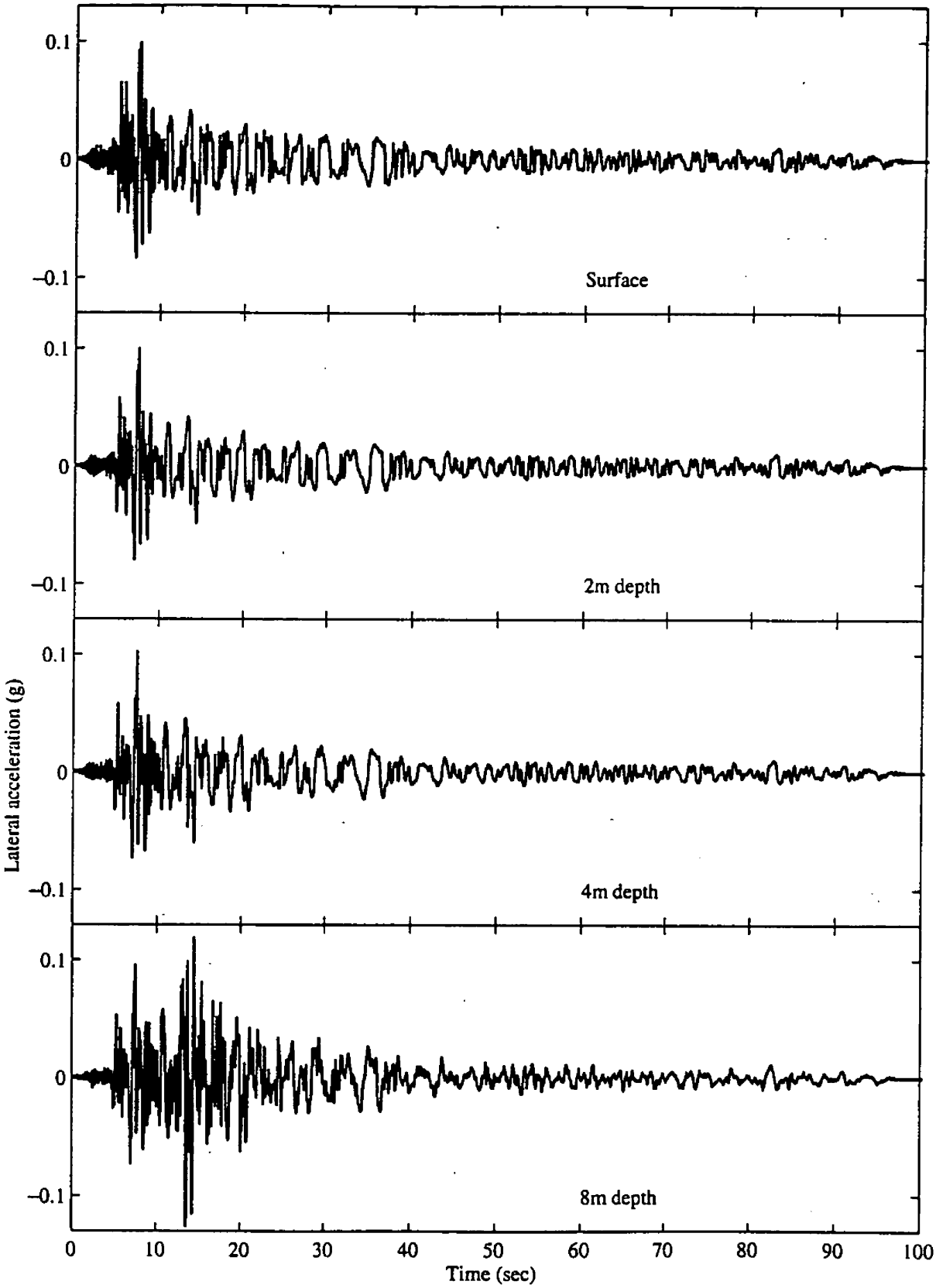

Fig. 5. Lateral acceleration time histories for Case MS1D (site response situation).

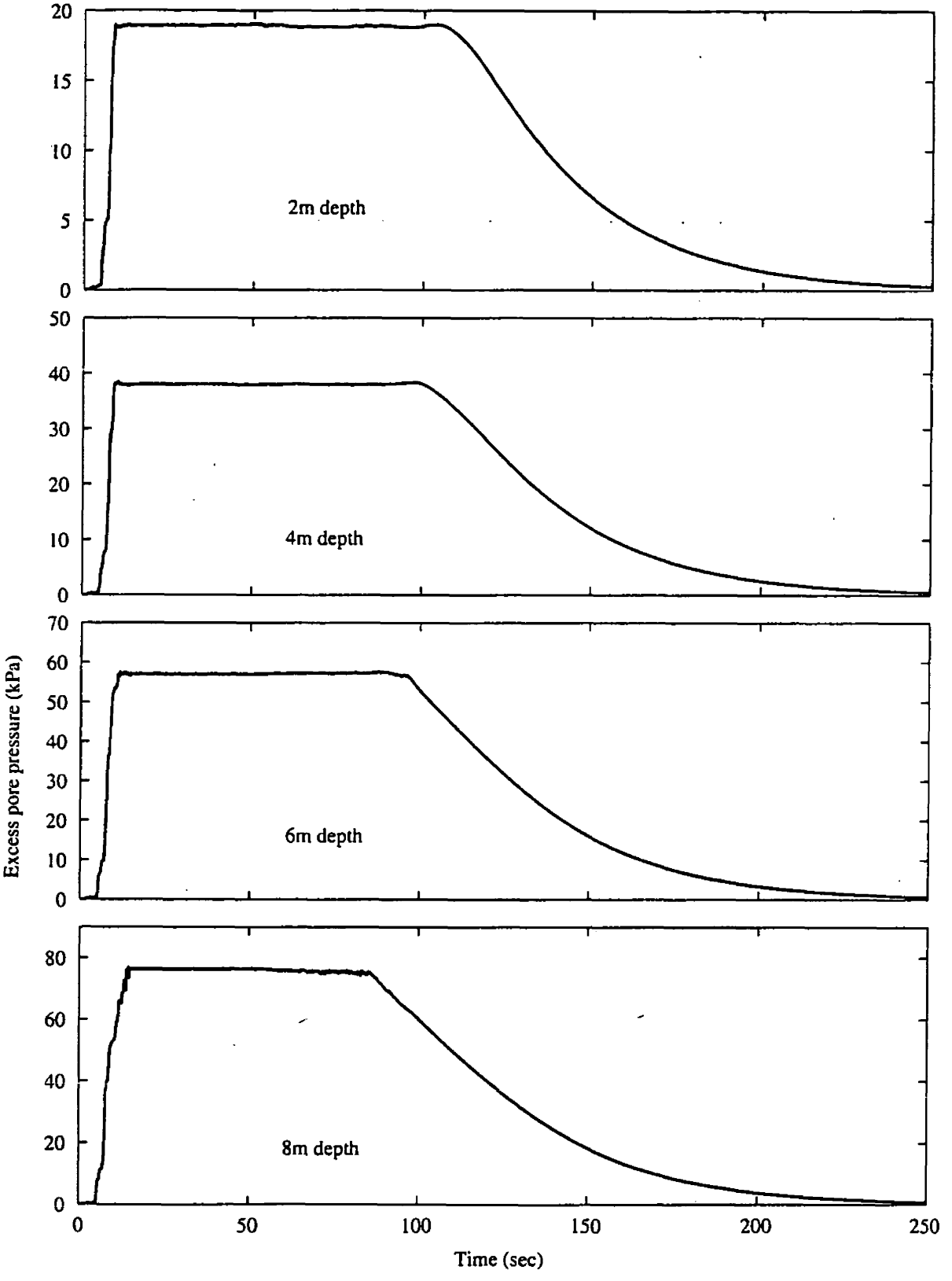

Fig. 6. Excess pore pressure time histories for Case MS1D (site response situation).

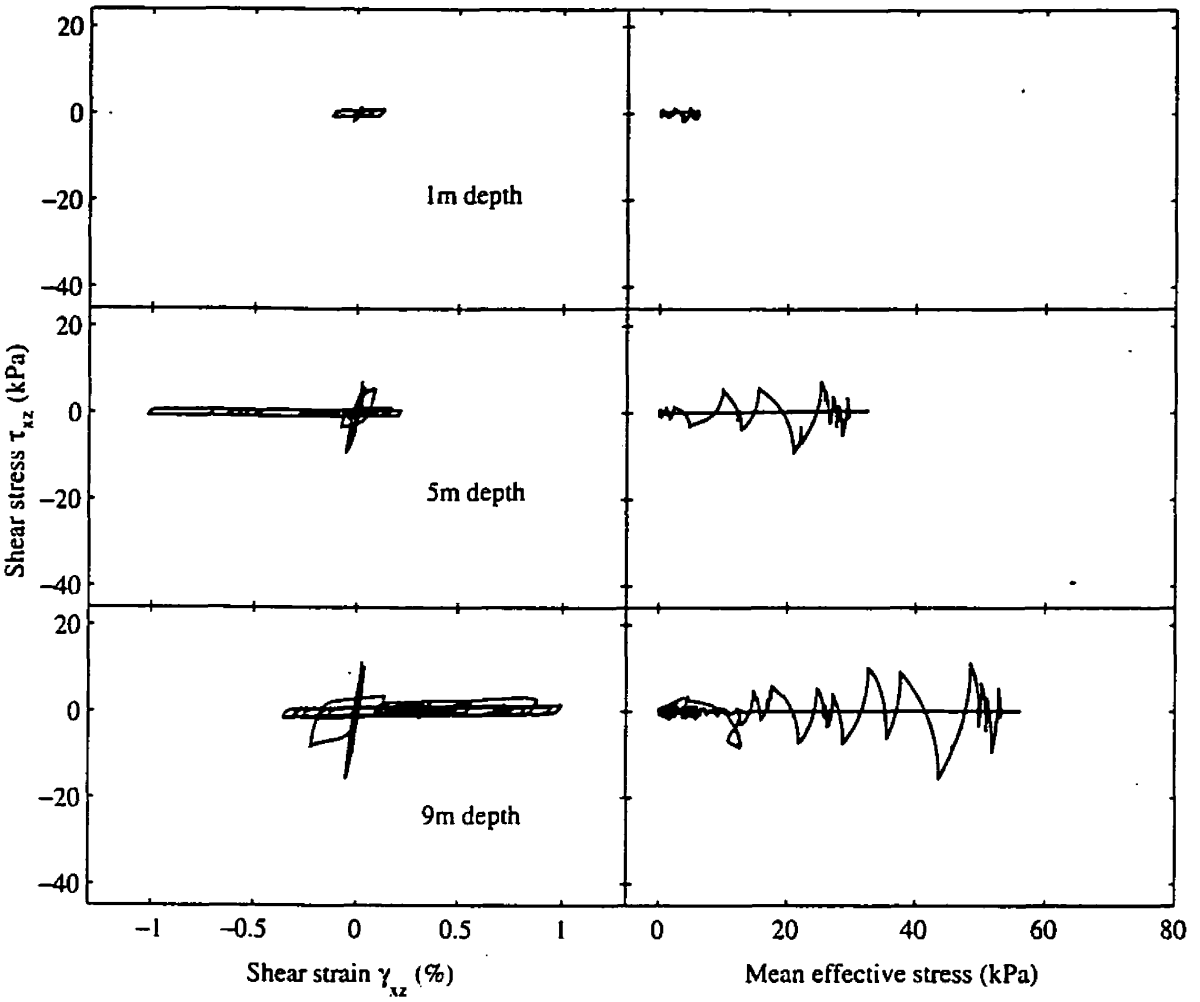

Fig. 7. Shear stress-strain and stress path at different depths for Case MS1D (site response situation).

7.4. *Permeability remediation*

Cases DG, DGL and DGL4 are the cases with high permeability (gravel). Figures 11 and 12 display u_e time histories at different depths under the foundation for cases DG and DGL4 respectively. Insignificant u_e was observed under the foundation up to the compacted depth. The dilative response, as seen in the stress paths (Fig. 13), was also manifested by pore pressure reduction instants (lower 2 graphs of Fig. 12).

8. High Fidelity Numerical Simulation

Each of the simulations discussed above required about 2 hours of computing time. However, the employed 75-elements mesh (Fig. 2) is rather coarse, and thus two more refined meshes (500-elements, Fig. 14(b) and 960-elements, Fig. 14(c)) were utilised for additional studies. Case DGL4 was analysed being the one resulting in the least settlement (0.02 m, Table 1). Figure 15 shows the u_e time histories for Case DGL4 with the 960-elements mesh. The u_e response (Fig. 15) was mostly

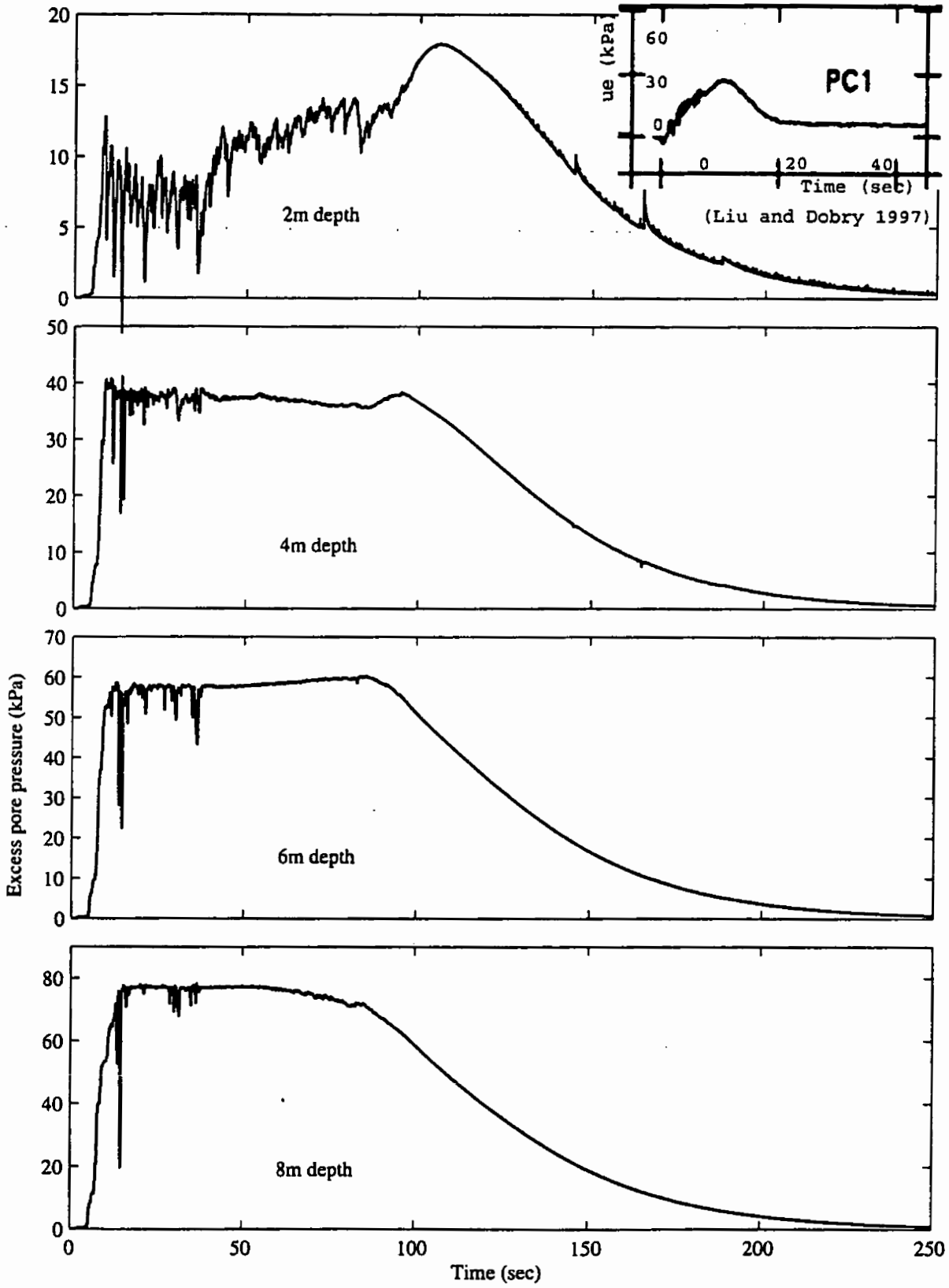

Fig. 8. Excess pore pressure time histories at different depths under foundation for Case MS.

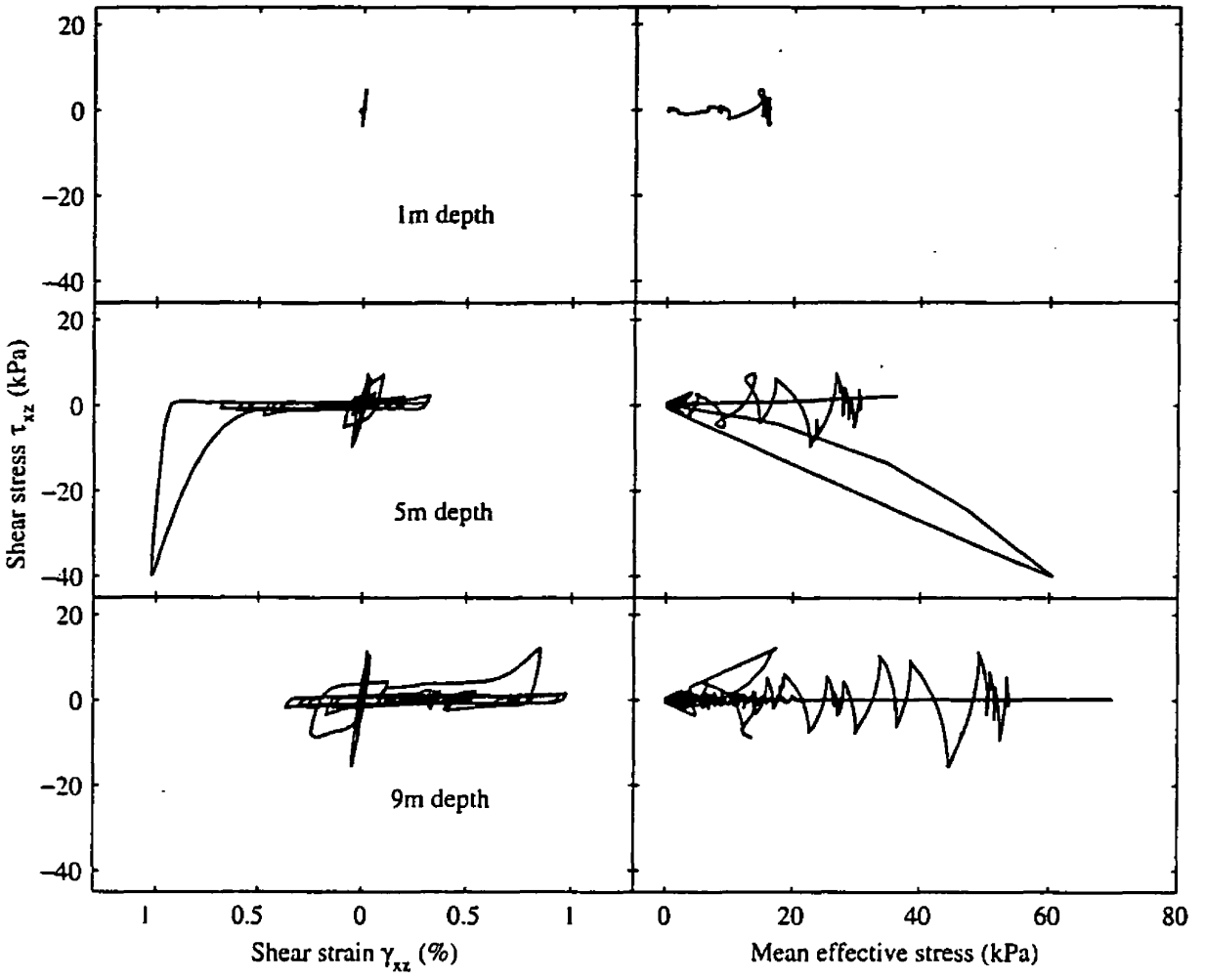

Fig. 9. Shear stress-strain and stress path at different depths (under foundation) for Case MS.

comparable to that obtained with the coarse mesh (Fig. 12), with the exception of less pronounced dilative response peaks (lower 2 graphs of Fig. 15).

Comparison of the foundation lateral acceleration with these three meshes (Case DGL4) is shown in Fig. 16. The foundation final settlement (Fig. 17) was 0.0335 m with the 500-elements mesh and 0.034 m with the 960-elements mesh. In this regard, the high fidelity meshes results in a more flexible system with additional final settlement of less than 0.001 m. As indicated in Figs. 16 and 17, the simulation results appear to have become essentially stable with the 500-element mesh and beyond.

9. Summary and Conclusions

A study was conducted to explore the influence of compaction and/or increased drainage on the liquefaction-induced settlement below an applied surface load. Within the scope of conducted simulations, high drainage was found to be effective in reducing settlement. In this regard, crude mesh simulations appeared useful in providing valuable qualitative insights.

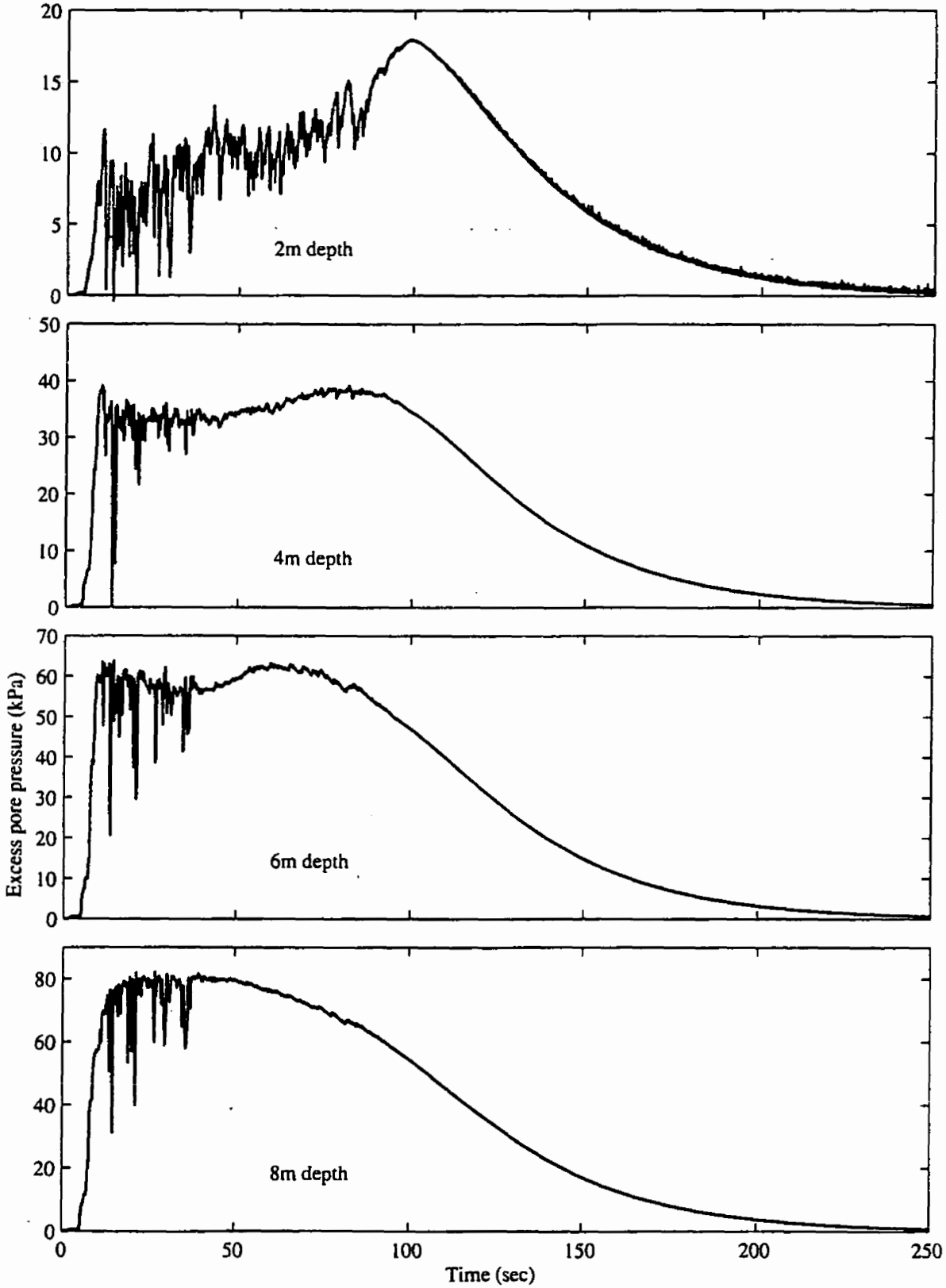

Fig. 10. Excess pore pressure time histories at different depths (under foundation) for Case DSL4.

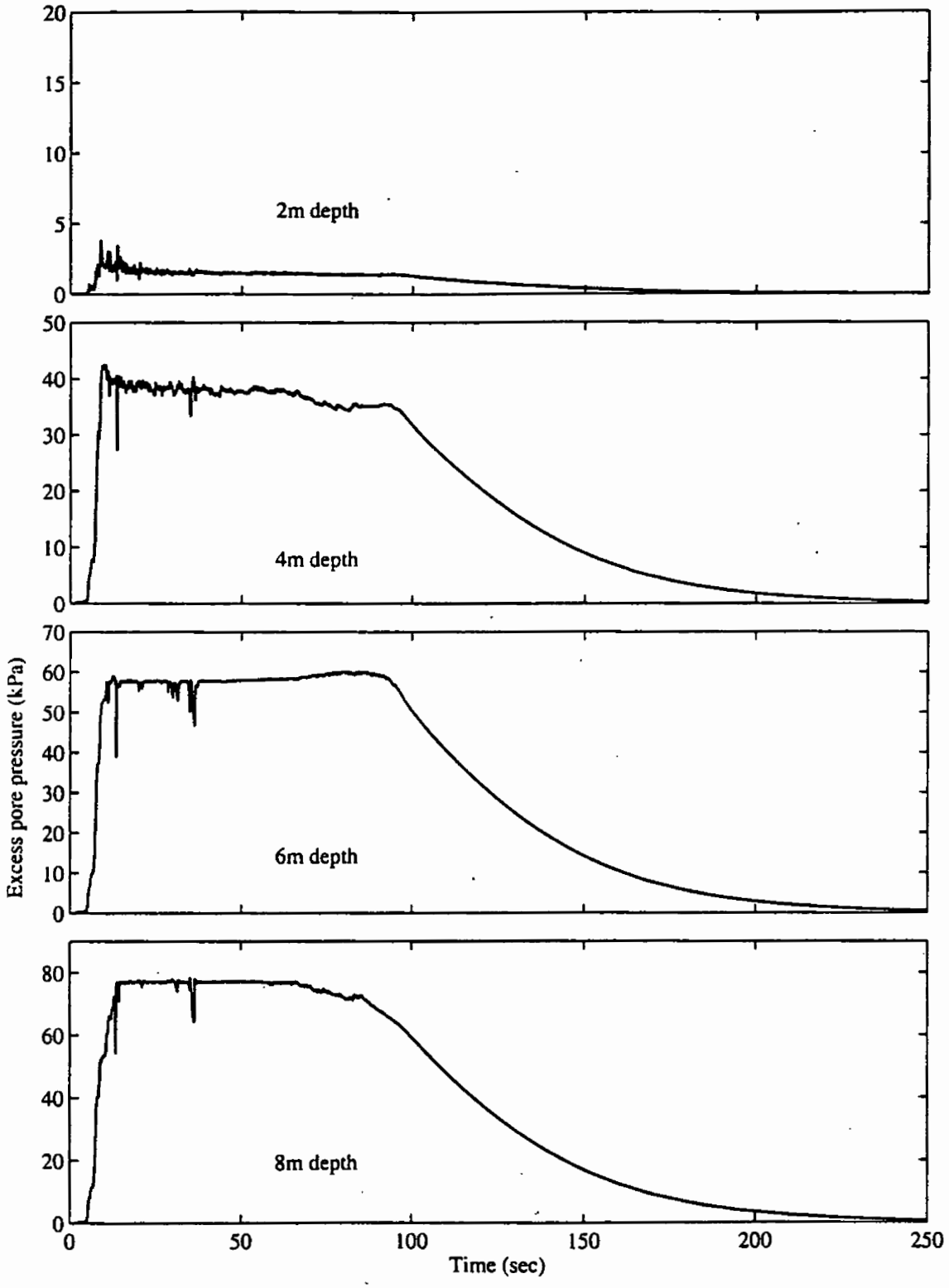

Fig. 11. Excess pore pressure time history at different depths (under foundation) for Case DG.

Such relatively simple simulations may be of great value in conducting "*what if*" scenarios, before execution of more elaborate numerical or physical model investigations. For instance, the reported study may be conveniently extended to explore the relative influence of changes in input excitation, permeability, shear

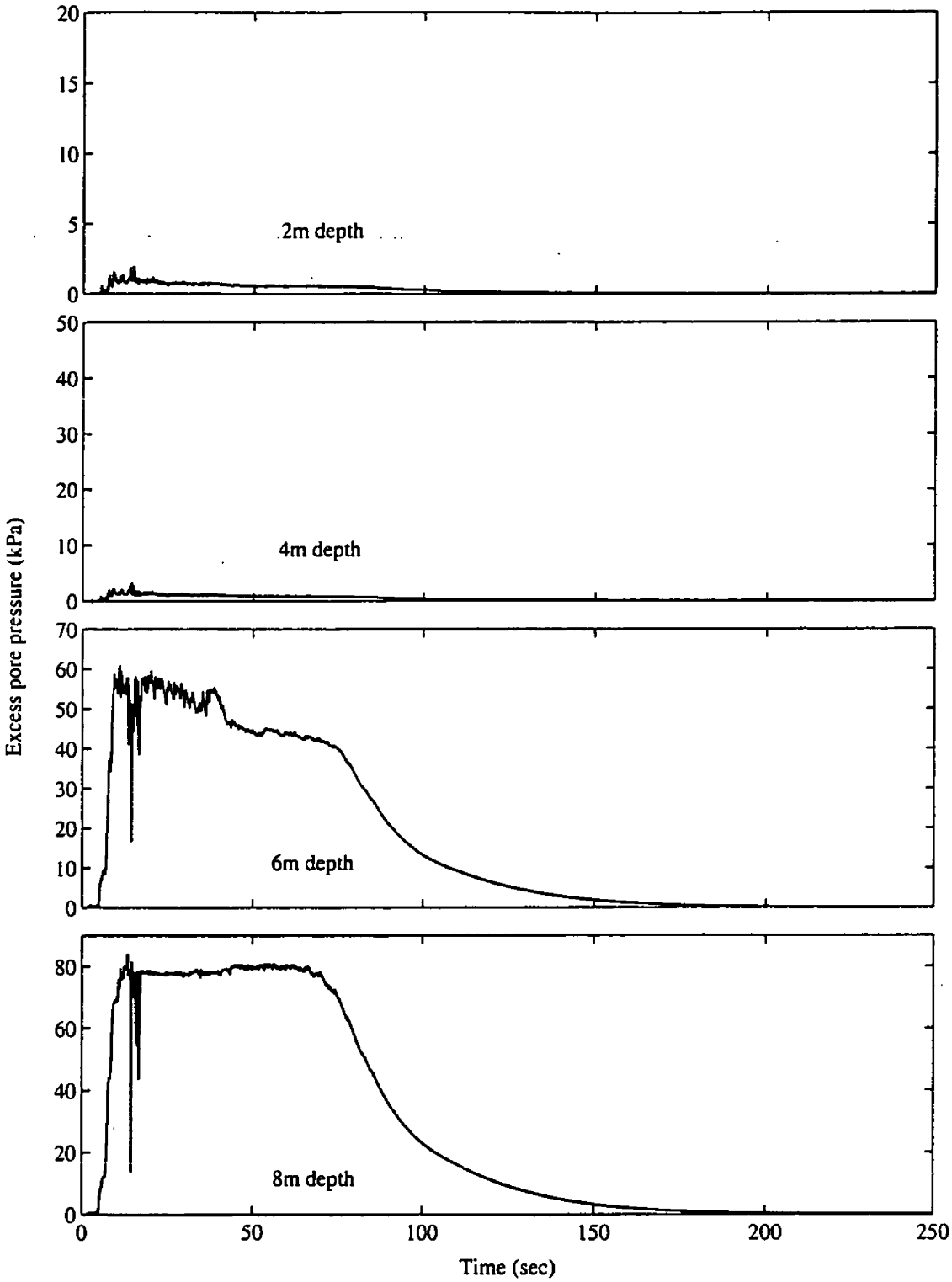

Fig. 12. Excess pore pressure time histories at different depths (under foundation) for Case DGL4.

stress-strain relationships (Fig. 20), surcharge stress and configuration, and extent of liquefaction-countermeasure remediation/treatment.

Appropriate user friendly interfaces (e.g. pilot effort, http://cyclic.ucsd.edu/cyclictp) can further simplify the process, and serve as a cost versus efficiency

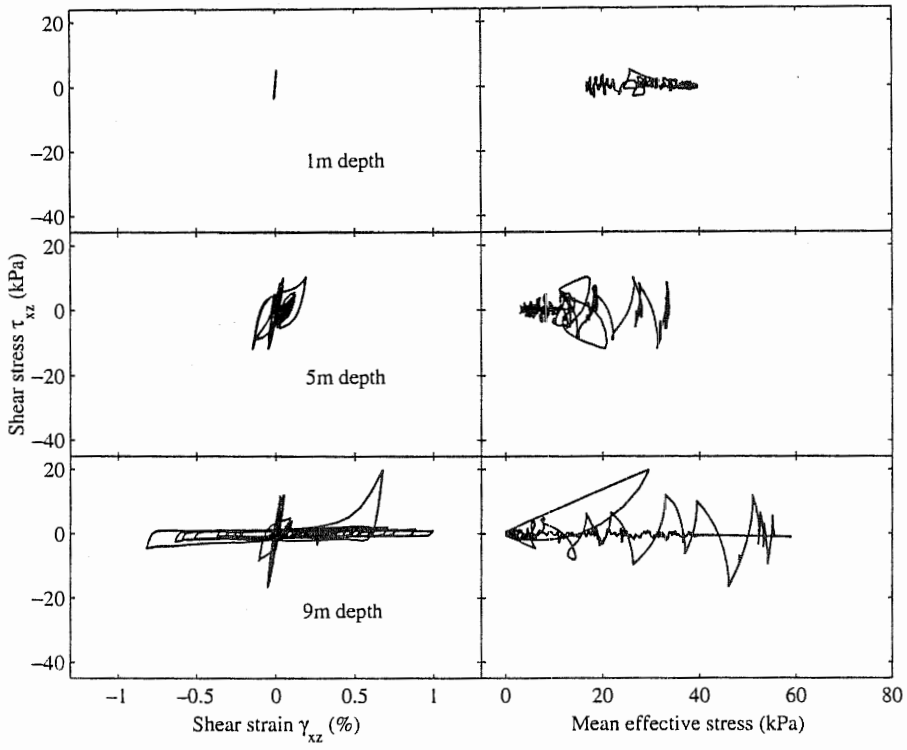

Fig. 13. Shear stress-strain and stress path at different depths (under foundation) for Case DGL4.

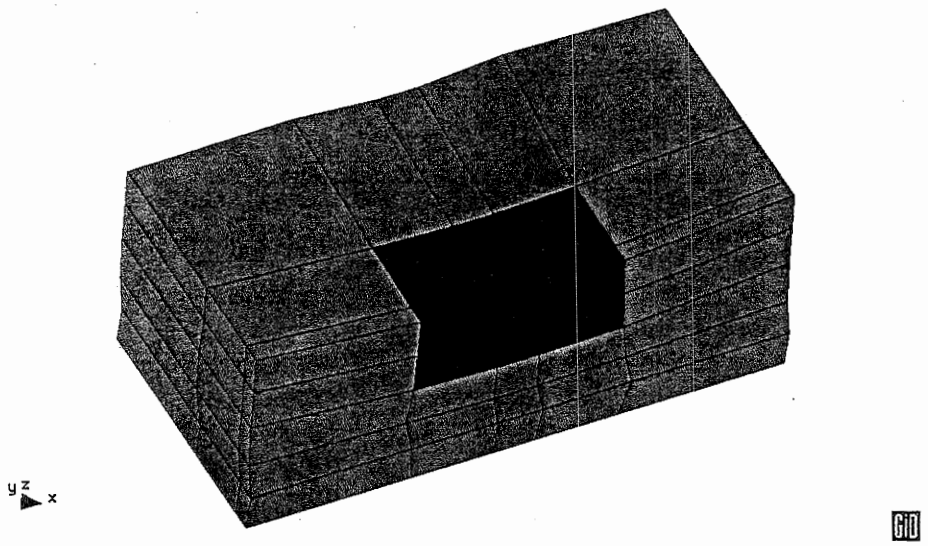

(a)

Fig. 14. Final deformed mesh (factor of 40) for Case DGL4 (dark zone represents remediated domain): (a) 75-element mesh; (b) 500-element mesh; (c) 960-element mesh.

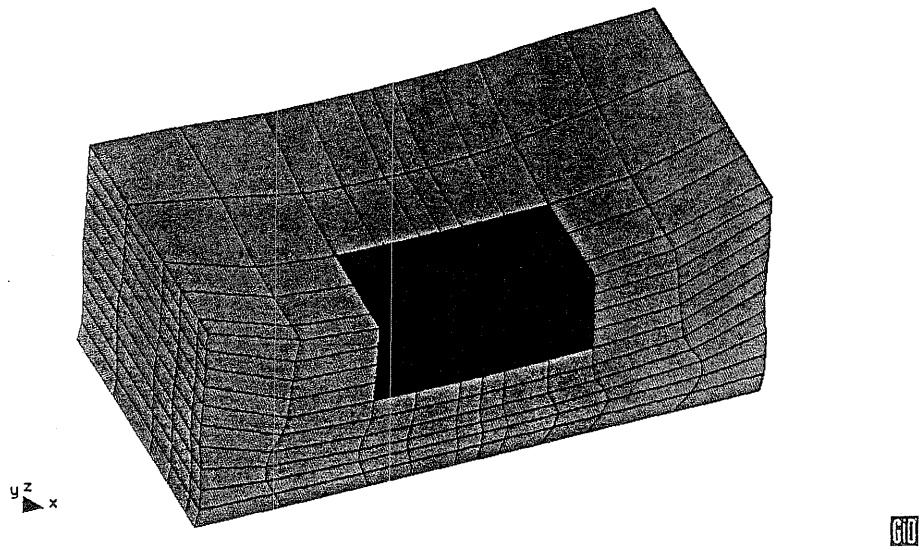

(b)

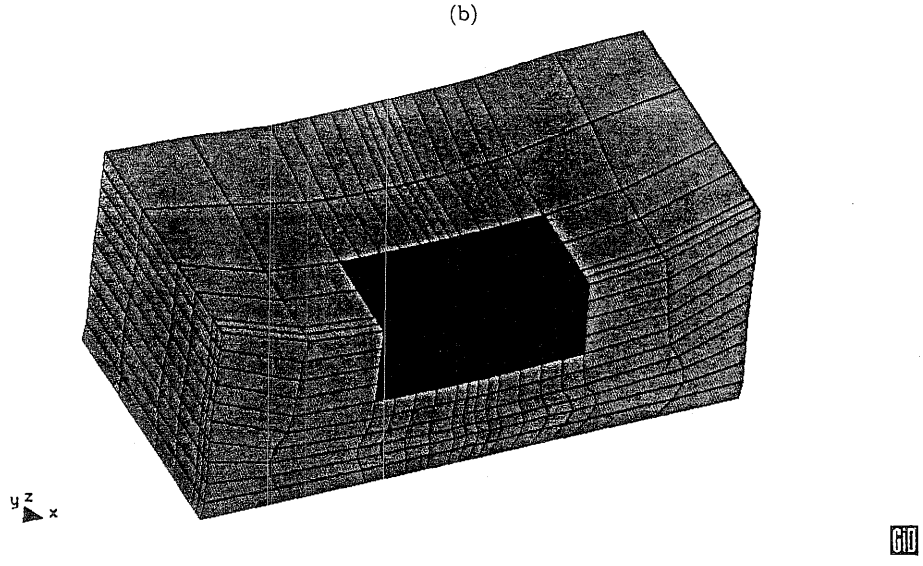

(c)

Fig. 14. (*Continued*)

decision-making tool (i.e. performance-based earthquake engineering framework for ground remediation). However, continued calibration of such a numerical framework based on experimentation/reconnaissance is a necessity. For instance, more accurate simulation of liquefaction-induced compaction and densification remains an area of challenges, which requires further research [Ragheb, 1994].

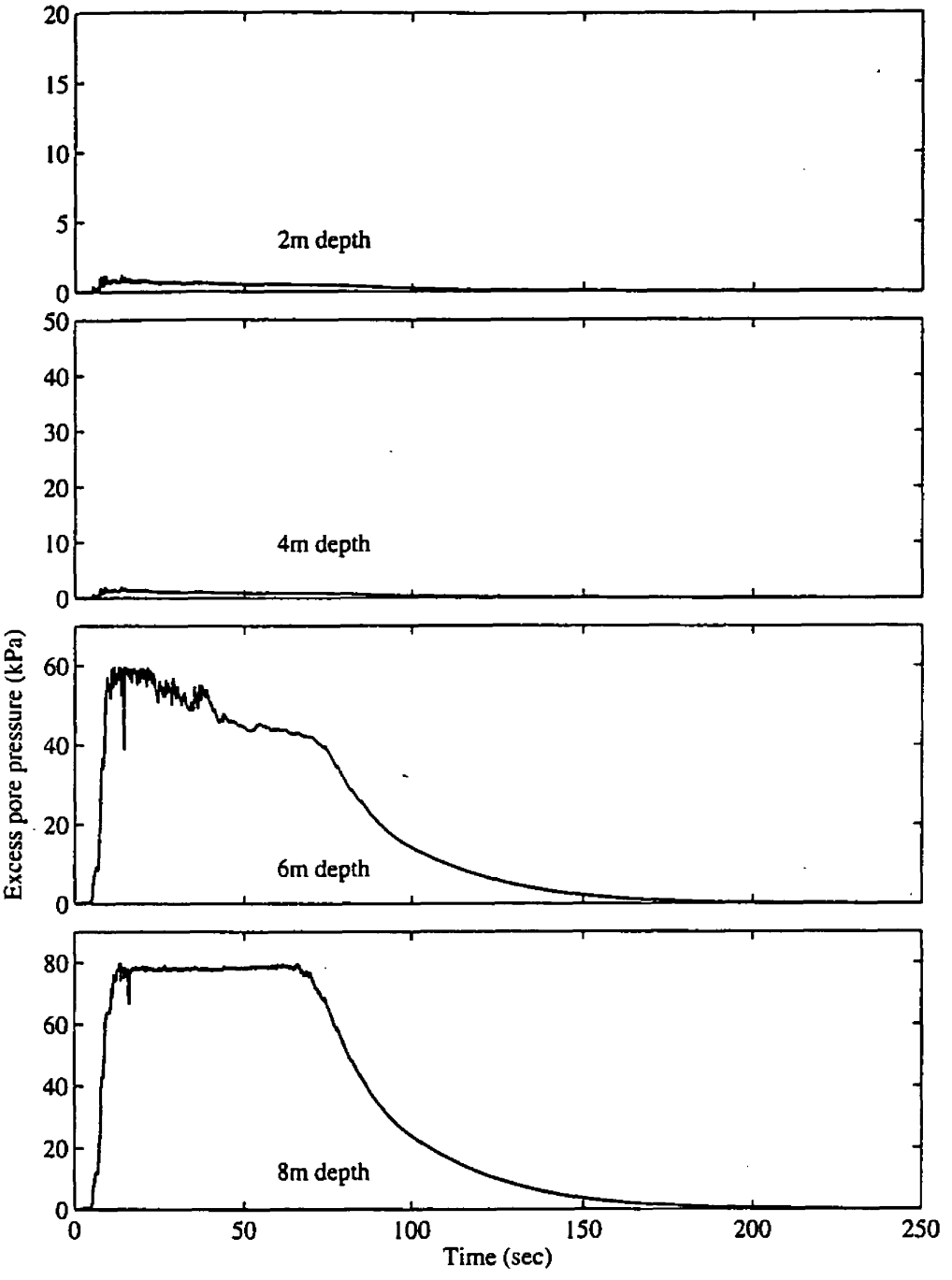

Fig. 15. Excess pore pressure time histories at different depths (under foundation) for Case DGL4 with the 960-element mesh.

Finally, high-fidelity 3D numerical studies were shown to provide more accurate estimates of liquefaction-induced settlements (on a relative scale). Such simulation environments are gradually becoming commonplace, and will be much facilitated through parallel and grid computing research [Lu, 2005; Lu, *et al.*, 2004; Peng, *et al.*, 2004].

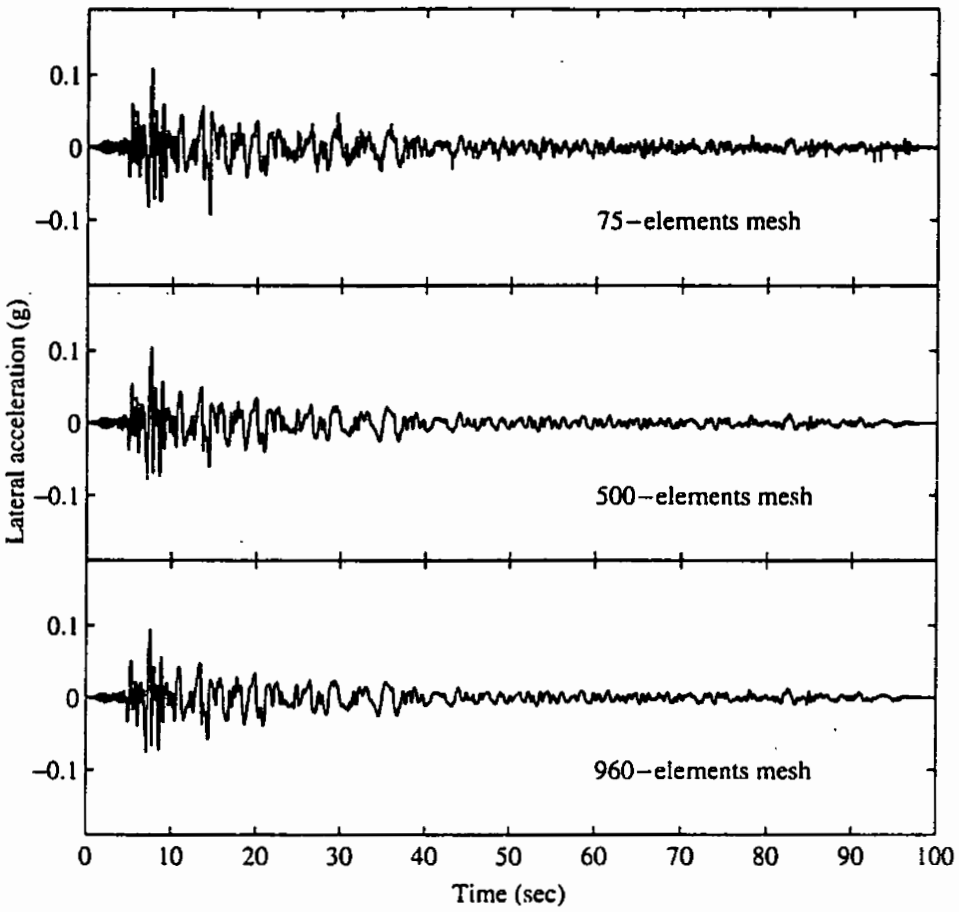

Fig. 16. Foundation lateral acceleration time histories for Case DGL4 with 3 different sizes of meshes.

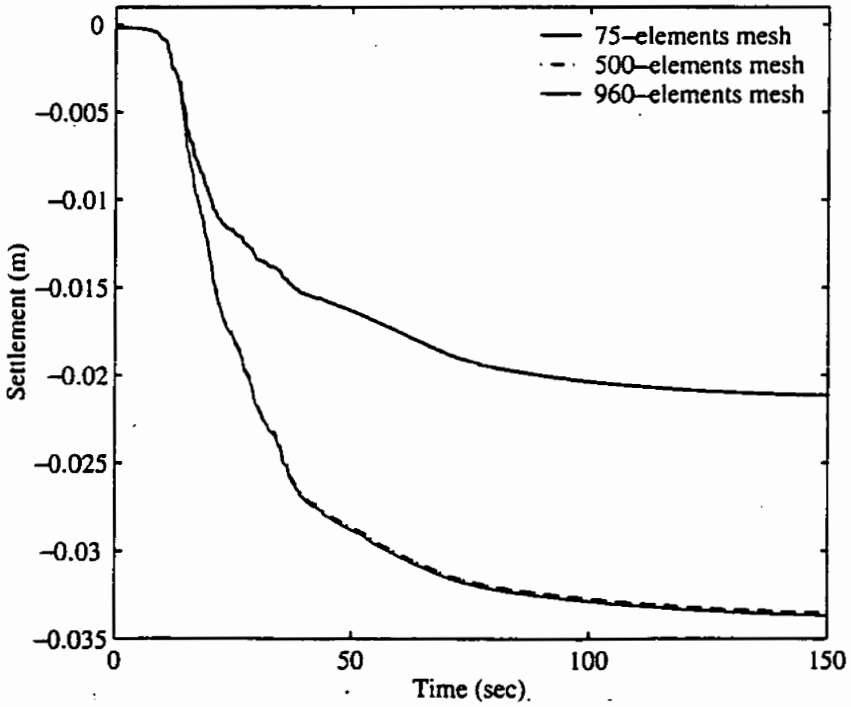

Fig. 17. Vertical displacement time histories of the foundation for Case DGL4.

Acknowledgements

The reported research was supported by the Pacific Earthquake Engineering Research (PEER) Center, under the National Science Foundation Award Number EEC-9701568, and by the National Science Foundation (Grants No. CMS0084616 and CMS0200510). This support is most appreciated.

Appendix: Computational Framework and Soil Model Properties

The saturated soil system is modelled as a two-phase material based on the Biot [1962] theory for porous media. A numerical formulation of this theory, known as *u-p* formulation (in which displacement of the soil skeleton u, and pore pressure p, are the primary unknowns, [Chan, 1988; Zienkiewicz *et al.*, 1990], was implemented [Parra, 1996; Yang, 2000; Yang and Elgamal, 2002]). This implementation is based on the following assumptions: Small deformation and rotation, density of the solid and fluid is constant in both time and space, porosity is locally homogeneous and constant with time, incompressibility of the soil grains, and equal accelerations for the solid and fluid phases.

The *u-p* formulation may be defined by [Chan, 1988]: (i) The equation of motion for the solid-fluid mixture, and (ii) the equation of mass conservation for the fluid phase, incorporating equation of motion for the fluid phase and Darcy's law. These two governing equations may be expressed in the following FE matrix form [Chan, 1988]:

$$\mathbf{M}\ddot{\mathbf{U}} + \int_{\Omega} \mathbf{B}^{\mathrm{T}} \sigma' \mathrm{d}\Omega + \mathbf{Q}\mathbf{p} - \mathbf{f}^{\mathbf{s}} = 0, \tag{1a}$$

$$\mathbf{Q}^{\mathrm{T}}\dot{\mathbf{U}} + \mathbf{S}\dot{\mathbf{p}} + \mathbf{H}\mathbf{p} - \mathbf{f}^{\mathbf{p}} = 0, \tag{1b}$$

where $\mathbf{M}$ is the total mass matrix, $\mathbf{U}$ the displacement vector, $\mathbf{B}$ the strain-displacement matrix, σ' the effective stress vector (determined by the soil constitutive model described below), $\mathbf{Q}$ the discrete gradient operator coupling the solid and fluid phases, $\mathbf{p}$ the pore pressure vector, $\mathbf{H}$ the permeability matrix, and $\mathbf{S}$ the compressibility matrix. The vectors $\mathbf{f}^{\mathbf{s}}$ and $\mathbf{f}^{\mathbf{p}}$ include the effects of body forces and prescribed boundary conditions for the solid-fluid mixture and the fluid phase respectively.

In Eq. 1(a) (equation of motion), the first term represents inertia force of the mixture, followed by internal force due to soil skeleton deformation, and internal force induced by pore-fluid pressure. In Eq. 1(b) (equation of mass conservation), the first two terms represent the rate of volume change for the soil skeleton and the fluid phase respectively, followed by the seepage rate of the pore fluid. Equations (1) are integrated in time using a single-step predictor multi-corrector scheme of the Newmark type [Chan, 1988; Parra, 1996]. The solution is obtained for each time step using the modified Newton-Raphson approach [Parra, 1996].

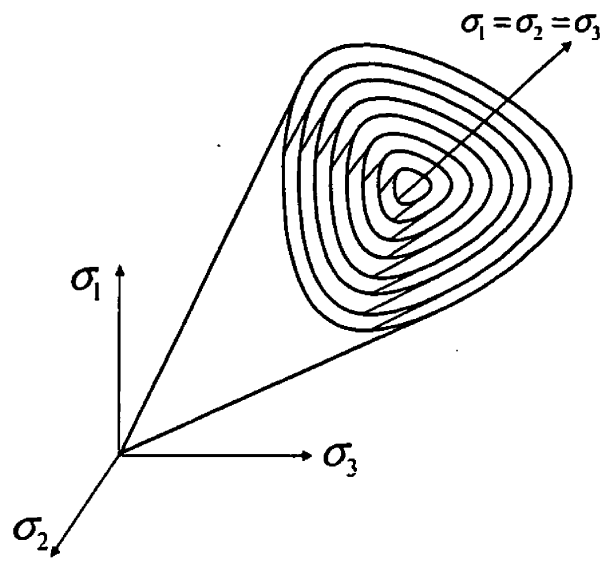

Fig. 18. Configuration of multi Lade-Duncan yield surfaces in principal stress space [Yang and Elgamal, 2004].

Soil constitutive model

The second term in Eq. 1(a) is defined by the soil stress-strain constitutive model. The FE program incorporates a soil constitutive model [Yang and Elgamal, 2004] based on the original multi-surface-plasticity theory for frictional cohesionless soils [Prevost, 1985]. This model was developed with emphasis on simulating the liquefaction-induced shear strain accumulation mechanism in clean medium-dense sands [Elgamal *et al.*, 2002a, 2002b, 2003; Yang and Elgamal, 2002; Yang *et al.*, 2003]. Special attention was given to the deviatoric-volumetric strain coupling (dilatancy) under cyclic loading, which causes increased shear stiffness and strength at large cyclic shear strain excursions (i.e. cyclic mobility).

The yield function (Fig. 18) was defined as the failure criteria proposed by Lade and Duncan [1975]:

$$f = \frac{I_1^3}{I_3} - \kappa_1 = 0, \tag{2}$$

where I_1 and I_3 are the first and third stress invariants respectively, and κ_1 (>27) is a parameter related to soil shear strength (or friction angle ϕ). In the context of multi-surface plasticity, a number of similar surfaces with a common apex form the hardening zone (Fig. 18). Each surface is associated with a constant plastic modulus. Conventionally [Prevost, 1985], the low-strain (elastic) moduli and plastic moduli are postulated to increase in proportion to the square root of mean effective confinement.

The flow rule is chosen so that the deviatoric component of flow $\mathbf{P}' = \mathbf{Q}'$ (associative flow rule in the deviatoric plane), and the volumetric component P'' defines the desired amount of dilation or contraction in accordance with experimental observations. Consequently, P'' defines the degree of non-associativity of the flow rule.

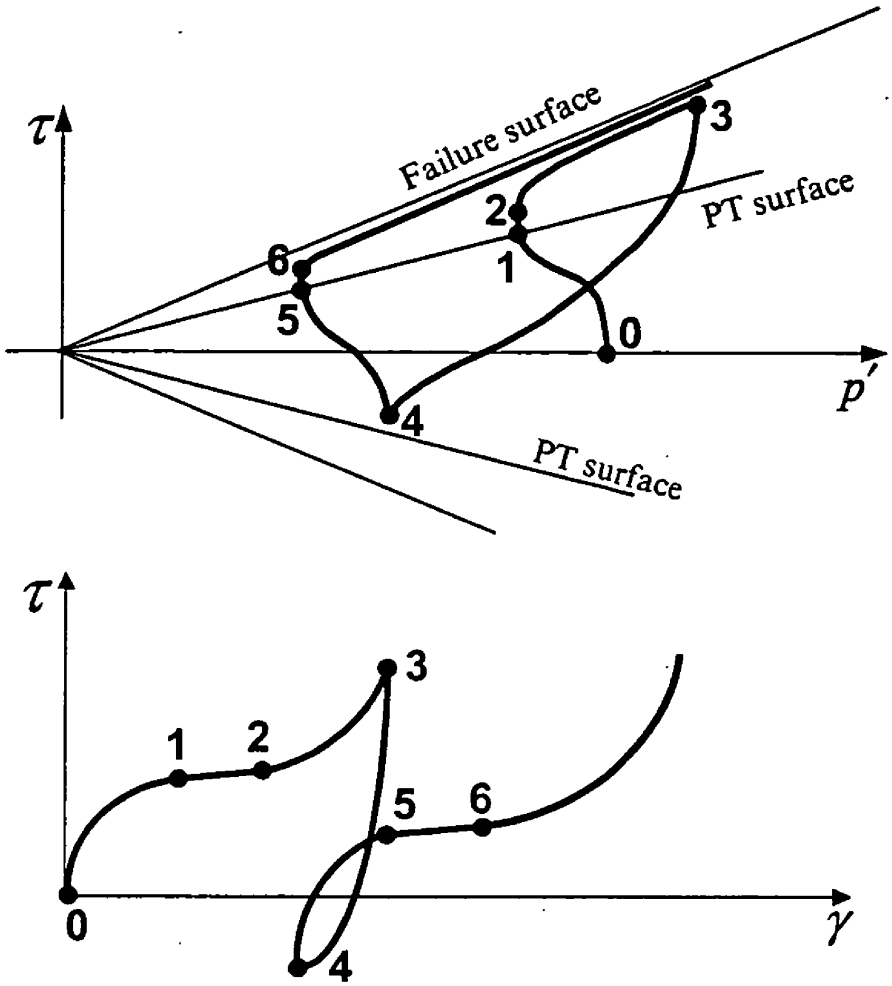

Fig. 19. Schematic showing the model undrained effective stress path and shear stress-strain response [Yang *et al.*, 2003].

The phase transformation (PT) surface [Ishihara *et al.*, 1975] defines the boundary between contractive and dilative behaviour under shear loading, assumed to be similar to the yield surfaces (Fig. 19). Along the PT surface, the stress ratio η is denoted as η_{PT}. Depending on the value of η with respect to η_{PT} and the sign of $\dot{\eta}$ (time rate of η), distinct contractive/dilative (dilatancy) behaviours are reproduced by specifying appropriate expressions for P'' [Yang *et al.*, 2003; Yang and Elgamal, 2004].

Thus, under undrained conditions, the adopted flow rule defines the following phases of soil response (Fig. 19):

(i) The contractive phase inside the PT surface ($\eta < \eta_{PT}$, phases 0–1 and 4–5), as well as outside during shear unloading ($\eta > \eta_{PT}$ with $\dot{\eta} < 0$, phase 3–4).
(ii) The dilative phase during shear loading, with the stress state outside the PT surface ($\eta > \eta_{PT}$ with $\dot{\eta} > 0$, phase 2–3), and
(iii) The neutral phase ($P'' = 0$, phase 1–2) between the contraction ($P'' > 0$, phase 0–1) and the dilation ($P'' < 0$, phase 2–3) phases. This phase is significant only at very low confinement (e.g. below 10 kPa for Nevada Sand), where

Table 2. Model parameters for medium sand and dense soils.

Parameters	Medium	Dense
Low-strain shear modulus G_r (at 80 kPa mean effective confinement)	78.5 MPa	135.0 MPa
Friction angle ϕ	31.4 degrees	40.0 degrees
(Fig. 19, phase 1–2)		
Liquefaction yield strain γ_y	0.5%	0
(Fig. 19, phase 0–1)		
Contraction parameter c_1	0.065	0.02
Contraction parameter c_2	400.0	400.0
(Fig. 19, phase 2–3)		
Phase Transformation angle ϕ_{PT}	26.5 degrees	26.0 degrees
Dilation parameter d_1	140.0	200.0
Dilation parameter d_2	1.0	1.0

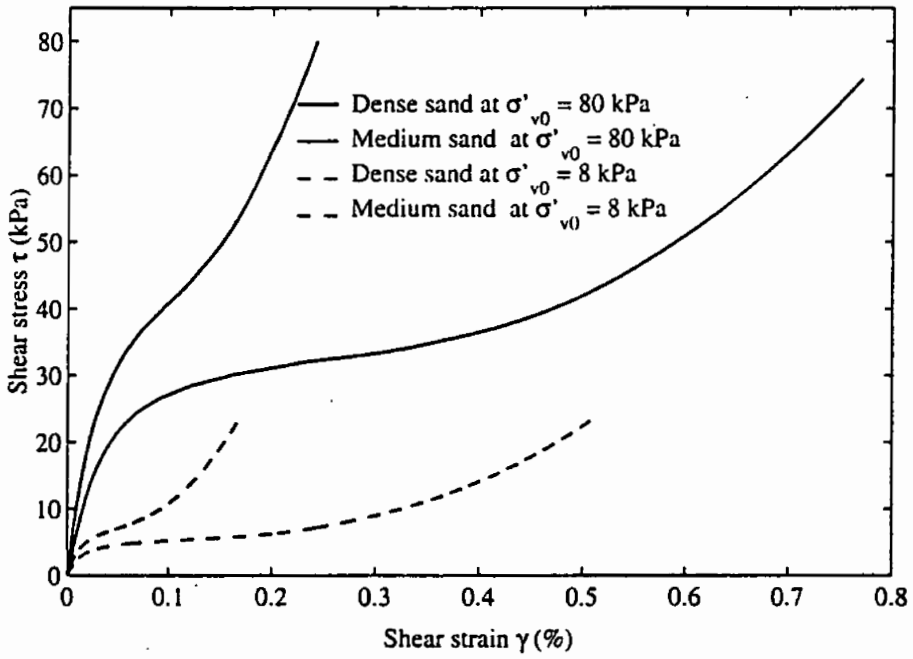

Fig. 20. Model shear stress-strain response under undrained conditions (initial vertical effective confinement $\sigma'_{v0} = 80$ and 8 kPa).

considerable permanent shear strain (γ_y) may accumulate with minimal change in shear stress [Yang *et al.*, 2003].

In summary, the main modelling parameters include (Table 2) standard dynamic soil properties such as low-strain shear modulus and friction angle, as well as parameters to control the dilatancy effects (phase transformation angle, contraction, and dilation), and the level of liquefaction-induced yield strain (γ_y). The constitutive model shear stress-strain response under undrained conditions is displayed in Fig. 20.

A purely deviatoric kinematic hardening rule is chosen according to [Prevost, 1985]:

$$p' = b\mu, \tag{3}$$

where μ is a deviatoric tensor defining the direction of translation and b is a scalar magnitude dictated by the consistency condition. In order to enhance computational efficiency, the direction of translation μ is defined by a new rule [Parra, 1996; Elgamal *et al.*, 2003], which maintains the original Mroz [1967] concept of conjugate-points contact. Thus, all yield surfaces may translate in stress space within the failure envelope.

References

Adachi, T., Iwai, S., Yasui, M. and Sato, Y. [1992] "Settlement of inclination of reinforced concrete buildings in Dagupan City due to liquefaction during the 1990 Philippines Earthquake," *Proceedings of the 10th World Conference on Earthquake Engineering*, A. A. Balkema (ed.), Madrid, Spain, July 19–25, **2**, 147–152.

Adalier, K., Elgamal, A.-W. and Martin, G. R. [1998] "Foundation liquefaction countermeasures for earth embankments," *Journal of Geotechnical and Geoenvironmental Engineering* **124**(6), 500–517.

Arulanandan, K. and Scott, R. F. [1993] "Verification of numerical procedures for the analysis of soil liquefaction problems," *Conference Proceedings* **1**, Balkema, Davis, CA.

Arulanandan, K. and Scott, R. F. [1994] "Verification of numerical procedures for the analysis of soil liquefaction problems," *Conference Proceedings* **2**, Balkema, Davis, CA.

Biot, M. A. [1962] "The mechanics of deformation and acoustic propagation in porous media," *Journal of Applied Physics* **33**(4), 1482–1498.

Borja, R. I. [2004] "Incorporating uncertainties in nonlinear soil properties into numerical models," *Proceedings of the International Workshop on Uncertainties in Nonlinear Soil Properties and their Impact on Modeling Dynamic Soil Response*, Pacific Earthquake Engineering Research Center (PEER), Berkeley, CA, March 18–19.

Bray, J. D., Sancio, R. B., Riemer, M. and Durgunoglu, H. T. [2004] "Liquefaction susceptibility of fine-grained soils," *Proceedings of the 11th International Conference on Soil Dynamics and Earthquake Engineering*, D. Doolin, A. Kammerer, T. Nogami, R. B. Seed and I. Towhata (eds.), Berkeley, CA, January 7–9, 1, 655–662.

Chan, A. H. C. [1988] "A unified finite element solution to static and dynamic problems in geomechanics," *PhD Thesis*, University College of Swansea, UK.

CIMNE [1999] *GiD Reference Manual*, http://gid.cimne.upc.es, International Center for Numerical Methods in Engineering, Barcelona, Spain.

Conte, J. P., Vijalapura, P. K. and Meghella, M. [2003] "Consistent finite-element response sensitivity analysis," *Journal of Engineering Mechanics* **129**(12), 1380–1393.

EERI [2000] "Kocaeli. Turkey, Earthquake of August 17, 1999 Reconnaissance Report," *Earthquake Spectra 16, Supplement A*, Earthquake Engineering Research Institute (EERI).

EERI [2001] "Chi-Chi, Taiwan, Earthquake of September 21, 1999, Reconnaissance Report," *Earthquake Spectra 17, Supplement A*, Earthquake Engineering Research Institute (EERI).

Elgamal, A., Lai, T., Yang, Z. and He, L. [2001] "Dynamic soil properties, seismic downhole arrays and applications in practice," *Proceedings of the 4th International Conference*

on Recent Advances in Geotechnical Earthquake Engineering and Soil Dynamics, S. Prakash (ed.), San Diego, CA, March 26–31.

Elgamal, A., Lu, J. and Yang, Z. [2004] "Data uncertainty for numerical simulation in geotechnical earthquake engineering," *Proceedings of the International Workshop on Uncertainties in Nonlinear Soil Properties and their Impact on Modeling Dynamic Soil Response*, Pacific Earthquake Engineering Research Center (PEER), Berkeley, CA, March 18–19.

Elgamal, A., Parra, E., Yang, Z. and Adalier, K. [2002a] "Numerical analysis of embankment foundation liquefaction countermeasures," *Journal of Earthquake Engineering* **6**(4), 447–471.

Elgamal, A., Yang, Z. and Parra, E. [2002b] "Computational modeling of cyclic mobility and post-liquefaction site response," *Soil Dynamics and Earthquake Engineering* **22**(4), 259–271.

Elgamal, A., Yang, Z., Parra, E. and Ragheb, A. [2003] "Modeling of cyclic mobility in saturated cohesionless soils," *International Journal of Plasticity* **19**(6), 883–905.

Gu, Q. and Conte, J. P. [2003] "Convergence studies in nonlinear finite element response sensitivity analysis," *Proceedings of the 9th International Conference on Applications of Statistics and Probability in Civil Engineering*, Berkeley, California, July 6–9.

Hausler, E. A. [2002] "Influence of ground improvement on settlement and liquefaction: A study based on field case history evidence and dynamic geotechnical centrifuge tests," *PhD Thesis*, Department of Civil Engineering, University of California, Berkeley, CA.

Holzer, T. L., Youd, T. L. and Hanks, T. C. [1989] "Dynamics of liquefaction during the 1987 Superstition Hills, California, Earthquake," *Science* **244**, 56–59.

Iai, S. [1991] "A strain space multiple mechanism model for cyclic behavior of sand and its application," *Earthquake Engineering Research Note No. 43*, Port and Harbor Research Institute, Ministry of Transport, Japan.

Ishihara, K., Alex, A. and Towhata, I. [1993] "Liquefaction-induced ground damage in Dagupan in the July 16, 1990 Luzon Earthquake," *Soils and Foundations* **33**(1), 133–154.

Ishihara, K., Tatsuoka, F. and Yasuda, S. [1975] "Undrained deformation and liquefaction of sand under cyclic stresses," *Soils and Foundations* **15**(1), 29–44.

Jeremic, B. [2004] Geowulf: http://sokocalo.engr.ucdavis.edu/~jeremic/GeoWulf/, University of California, Davis, Davis, CA.

JGS [1996] Special Issue on *Geotechnical Aspects of the January 17, 1995 Hyogoken-Nanbu Earthquake, Soils and Foundations* (Tokyo, Japan), Japanese Geotechnical Society.

JGS [1998] Special Issue on *Geotechnical Aspects of the January 17, 1995 Hyogoken-Nanbu Earthquake, No. 2, Soils and Foundations* (Tokyo, Japan), Japanese Geotechnical Society.

Ju, S. H. [2004] "Three-dimensional analyses of wave barriers for reduction of train-induced vibrations," *Journal of Geotechnical and Geoenvironmental Engineering* **130**(7), 740–748.

Kishida, H. [1966] "Damage to reinforced concrete buildings in Niigata City with special reference to foundation engineering," *Soils and Foundations* **6**(1), 71–88.

Kokusho, T. [1999] "Water film in liquefied sand and its effect on lateral spread," *Journal of Geotechnical and Geoenvironmental Engineering*, ASCE **125**(10), 817–826.

Kramer, S. L. [1996] *Geotechnical Earthquake Engineering*, Prentice Hall, Upper Saddle River, NJ.

Kramer, S. L. and Elgamal, A. [2001] "Modeling soil liquefaction hazards for performance-based earthquake engineering," *PEER Report 2001/13*, Pacific Earthquake Engineering Research Center (PEER), Berkeley, CA.

Lade, P. V. and Duncan, J. M. [1975] "Elastoplastic stress-strain theory for cohesionless soil," *Journal of Geotechnical Engineering Division,* ASCE **101**(GT10), 1037–1053.

Liu, L. and Dobry, R. [1997] "Seismic response of shallow foundation on liquefiable sand," *Journal of Geotechnical and Geoenvironmental Engineering,* ASCE **123**(6), 557–567.

Lu, J. [2005] "Parallel finite element modeling of earthquake site response and liquefaction," *PhD Thesis* (in progress), Department of Structural Engineering, University of California, San Diego, La Jolla, CA.

Lu, J., He, L., Yang, Z., Abdoun, T. and Elgamal, A. [2004] "Three-dimensional finite element analysis of dynamic pile behavior in liquefied ground," *Proceedings of the 11th International Conference on Soil Dynamics and Earthquake Engineering*, D. Doolin, A. Kammerer, T. Nogami, R. B. Seed and I. Towhata (eds.), Berkeley, CA, January 7–9, **1**, 144–148.

Malvick, E. J., Kutter, B. L., Boulanger, R. W. and Feigenbaum1, H. P. [2004] "Post-shaking failure of sand slope in centrifuge test," *Proceedings of the 11th International Conference on Soil Dynamics and Earthquake Engineering*, D. Doolin, A. Kammerer, T. Nogami, R. B. Seed and I. Towhata (eds.), Berkeley, CA, January 7–9, **2**.

Manzari, M. [2004] "Large deformation analysis in liquefaction problems," *Proceedings of the 17th ASCE Engineering Mechanics Division Conference*, Newark, Delaware, June 13–16.

McKenna, F. and Fenves, G. L. [2001] *OpenSees Manual*, PEER Center, http://opensees.berkeley.edu.

Mroz, Z. [1967] "On the description of anisotropic work hardening," *Journal of Mechanics and Physics of Solids* **15**, 163–175.

Ohsaki, Y. [1966] "Niigata Earthquake, 1964 building damage and soil condition," *Soils and Foundations* **6**(2), 14–37.

Parra, E. [1996] "Numerical modeling of liquefaction and lateral ground deformation including cyclic mobility and dilation response in soil systems," *PhD Thesis*, Department of Civil Engineering, Rensselaer Polytechnic Institute, Troy, NY.

Pecker, A., Prevost, J. H. and Dormieux, L. [2001] "Analysis of pore pressure generation and dissipation in cohesionless materials during seismic loading," *Journal of Earthquake Engineering* **5**(4), 441–464.

Peng, J., Liu, D. and Law, K. H. [2003] "An online data access system for a finite element program," *Advances in Engineering Software* **34**(3), 163–181.

Peng, J., Lu, J., Law, K. H. and Elgamal, A. [2004] "ParCYCLIC: Finite element modeling of earthquake liquefaction response on parallel computers," *International Journal for Numerical and Analytical Methods in Geomechanics* **28**(12), 1207–1232.

Prevost, J. H. [1985] "A simple plasticity theory for frictional cohesionless soils," *Soil Dynamics and Earthquake Engineering* **4**(1), 9–17.

Ragheb, A. M. [1994] "Numerical analysis of seismically induced deformations," In *Saturated Granular Soil Strata*, PhD Thesis, Department of Civil Engineering, Rensselaer Polytechnic Institute, Troy, NY.

Seed, H. B. and Idriss, I. M. [1967] "Analysis of soil liquefaction: Niigata Earthquake," *Journal of Soil Mechanics and Foundations Division,* ASCE **93**(3), 83–108.

Sharp, M. K., Dobry, R. and Abdoun, T. [2003] "Liquefaction centrifuge modeling of sands of different permeability," *Journal of Geotechnical and Geoenvironmental Engineering,* ASCE **129**(12), 1083–1091.

Tokimatsu, K., Kojima, H., Kuwayama, S. and Midorikawa, S. [1994] "Liquefaction-induced damages to buildings in 1990 Luzon Earthquake," *Journal of Geotechnical Engineering,* ASCE **120**(2), 290–307.

Tokimatsu, K., Midorikawa, S., Tamura, S., Kuwayama, S. and Abe, A. [1991] "Preliminary report on the geotechnical aspects of the Philippine Earthquake of July 16, 1990," *Proceedings of the 2nd International Conference on Recent Advances in Geotechnical Earthquake Engineering and Soil Dynamics*, University of Missouri-Rolla, **1**, 357–364.

Yang, Z. [2000] *Numerical Modeling of Earthquake Site Response Including Dilation and Liquefaction*, PhD Thesis, Department of Civil Engineering and Engineering Mechanics, Columbia University, New York, NY.

Yang, Z. and Elgamal, A. [2002] "Influence of permeability on liquefaction-induced shear deformation," *Journal of Engineering Mechanics,* ASCE **128**(7), 720–729.

Yang, Z. and Elgamal, A. [2004] "A cyclic plasticity constitutive model for cohesionless soils," Submitted for journal publication.

Yang, Z., Elgamal, A. and Parra, E. [2003] "A computational model for cyclic mobility and associated shear deformation," *J. Geotechnical and Geoenvironmental Engineering* **129**(12), 1119–1127.

Yoshimi, Y. and Tokimatsu, K. [1977] "Settlement of buildings on saturated sand during earthquakes," *Soils and Foundations* **17**(1), 23–38.

Youd, T. L. and Holzer, T. L. [1994] "Piezometer performance at the wildlife liquefaction site," *Journal of Geotechnical Engineering* **120**(6), 975–995.

Zeghal, M. and Elgamal, A. [1994] "Analysis of site liquefaction using earthquake records," *Journal of Geotechnical Engineering* **120**(6), 996–1017.

Zienkiewicz, O. C., Chan, A. H. C., Pastor, M., Paul, D. K. and Shiomi, T. [1990] "Static and dynamic behavior of soils: A rational approach to quantitative solutions: I. Fully saturated problems," *Proceedings of the Royal Society of London* **A429**, 285–309.